

Atom dynamics in multiple Laguerre-Gaussian beams

L. Allen, M. Babiker, W. K. Lai, and V. E. Lembessis

Department of Physics, University of Essex, Colchester, Essex C04 3SQ, United Kingdom

(Received 10 April 1996)

The leading radiation forces acting on an atom or ion subject to linearly polarized Laguerre-Gaussian (LG) light are studied. Particular emphasis is laid on the orbital angular momentum effects associated with LG light. The optical Bloch equations appropriate for the adiabatic approximation are derived and used to evaluate the forces and associated torque governing the atomic motion. The steady-state dynamics of the atom are explored for atoms subject to a single beam and multiple independent counterpropagating beams. The main features responsible for the dynamics of the atom, together with the dipole potentials characteristic of Laguerre-Gaussian light, are identified and discussed. The theory is illustrated by the numerical integration of the equation of motion for Mg^+ ions in various beam configurations. This yields information on trajectories, velocity evolution, and vibrational frequencies at potential minima. Interesting effects involving a reciprocal interplay between motions in orthogonal directions are demonstrated. Such features are purely dependent on the orbital angular momentum property of the light. Their possible use in controlling atomic motion is investigated. [S1050-2947(96)07210-1]

PACS number(s): 32.80.Pj, 42.50.Vk

I. INTRODUCTION

The radiation forces associated with the near-resonant interaction of laser light with atoms and ions have been the subject of intensive theoretical and experimental study [1–4] since the basic mechanisms were first recognized [5]. The simplest features can be described with reference to a two-level atom subject to an electromagnetic wave. Near resonance, such an atom experiences two distinct forces: a dissipative force that arises from the absorption of the light by the atom followed by its spontaneous emission and a dipole force that arises from the nonuniformity of the field distribution. These basic forces underpin many of the applications involving the manipulation of atoms by lasers in a variety of beam configurations. The dissipative force has been exploited in cooling the atomic motion [6] and the dipole force used for trapping [7].

Much of the previous theoretical work in this context has assumed plane-wave modes. However, the demonstration that Laguerre-Gaussian (LG) laser beams possess well-defined orbital angular momentum $l\hbar$ [8,9] that originates in the azimuthal phase dependence of the field distribution has aroused new interest in the basic physics. The orbital angular momentum of LG beams is quite distinct from the spin angular momentum associated with circularly polarized light and can occur in linearly polarized LG modes. A circularly polarized LG beam possesses spin angular momentum as well as orbital angular momentum and can exhibit features involving spin-orbit coupling [10]. In our recent work [11] we presented a theory for the motion of a two-level atom in a Laguerre-Gaussian beam with spontaneous emission and saturation effects taken into account heuristically. The results found were in the form of an azimuthal shift in the atomic resonance and a torque about the beam axis.

The purpose of this paper is twofold: first, to present a more rigorous theory for the forces due to LG light and their effects on a two-level atom and, second, we extend our investigations on the orbital angular momentum effects beyond

the one beam case in order to explore more fully the effects of the orbital angular momentum on atomic motion. The theory is developed in terms of the optical Bloch equations (OBEs) [1,12,13] that allow the *ab initio* inclusion of relaxation effects and naturally incorporate saturation phenomena. The solution of the OBEs in the adiabatic, or constant velocity, approximation lends insight into the time evolution of angular momentum effects for an atom in a LG beam. In the long-time limit, these solutions lead directly to the steady-state results for the dissipative and dipole forces due to a LG beam.

In Sec. II we set up the density-matrix formalism appropriate for a two-level atom interacting with Laguerre-Gaussian light. In the adiabatic approximation this leads to the optical Bloch equations that formally enable the calculation of the average mechanical force (defined as the rate of change of the atomic momentum). We argue that as the concept of force is a classical one, the rate of change of momentum can only be interpreted as a force for elapsed times greater than the spontaneous decay time Γ^{-1} , where time is measured from the instant the light beam is switched on [1]. With this restriction, we solve the OBEs to determine the evolution of the average “force” components from the instant the LG beam is switched on. It is possible to examine the time evolution in a number of limits, but we discuss primarily the steady state. Further insight into the nature of the forces is gained by the numerical solution of the optical Bloch equations for a typical set of parameters. In Sec. III we give an analysis of the steady-state dissipative and dipole forces for various beam configurations and identify the features directly attributable to the angular momentum of the LG beams. The motion of a Mg^+ ion in counterpropagating LG fields is described in Sec. IV after solving the equation of motion numerically. The results demonstrate the effects of a characteristic torque and of reciprocating forces between axial and azimuthal motions. Section V contains conclusions and further comment.

II. FORMALISM

We wish to examine the evolution of the average force acting on a two-level atom or ion, henceforth referred to as the atom, due to its interaction with light. The light is in the form of a coherent beam with a complex amplitude α and has a LG distribution [8]. An appropriate Hamiltonian is given by

$$H = H_A + H_F + H_{\text{int}}, \quad (1)$$

where H_A and H_F are the unperturbed Hamiltonians for the atom and field, respectively, and are

$$H_A = \frac{\mathbf{P}^2}{2M} + \hbar \omega_0 \pi^\dagger \pi, \quad (2)$$

$$H_F = \hbar \omega a^\dagger a. \quad (3)$$

Here \mathbf{P} is the center-of-mass momentum operator and π and π^\dagger are the atomic lowering and raising operators; M is the mass of the atom and ω_0 is the atomic transition frequency. In Eq. (3) a and a^\dagger are the annihilation and creation operators and ω is the frequency of the field.

The interaction Hamiltonian H_{int} in Eq. (1) describes the coupling of the atom to the electromagnetic field and is given in the electric dipole approximation by

$$H_{\text{int}} = -\mathbf{d} \cdot \mathbf{E}(\mathbf{R}), \quad (4)$$

where \mathbf{d} is the atomic dipole moment operator and $\mathbf{E}(\mathbf{R})$ is the electric field evaluated at the position \mathbf{R} of the atom. The atomic dipole moment operator may be written as

$$\mathbf{d} = \mathbf{D}_{12}(\pi + \pi^\dagger), \quad (5)$$

where \mathbf{D}_{12} is the dipole matrix element of the atomic transition. The electric-field vector associated with a Laguerre-Gaussian mode propagating along the z axis is given by

$$\mathbf{E}(\mathbf{R}) = i[a \hat{\boldsymbol{\epsilon}} \mathcal{E}_{klp}(\mathbf{R}) e^{i\Theta_{klp}(\mathbf{R})} - \text{H.c.}], \quad (6)$$

where $\hat{\boldsymbol{\epsilon}}$ is a polarization vector in the x - y plane. The electric field of a LG beam has a small vector component along the z axis [11,14], which we have ignored. It can easily be shown that the ignored term is of the order λ/w_0 relative to the principal component along $\hat{\boldsymbol{\epsilon}}$ [11]. In Eq. (6) $\mathcal{E}_{klp}(\mathbf{R})$ and $\Theta_{klp}(\mathbf{R})$ are, respectively, the mode amplitude and phase of the electric field, which may be written as [11,14]

$$\mathcal{E}_{klp}(\mathbf{R}) = \mathcal{E}_{k00} \frac{C_{lp}}{(1+z^2/z_R^2)^{1/2}} \left(\frac{\sqrt{2}r}{w(z)} \right)^{|l|} L_p^{|l|} \left(\frac{2r^2}{w^2(z)} \right) e^{-r^2/w^2(z)}, \quad (7)$$

$$\Theta_{klp}(\mathbf{R}) = \frac{kr^2z}{2(z^2+z_R^2)} + l\phi + (2p+l+1)\tan^{-1}(z/z_R) + kz. \quad (8)$$

Here $C_{lp} = \sqrt{p!/(|l|+p)!}$ is a normalization constant; $w(z)$ is given by $w^2(z) = 2(z^2+z_R^2)/kz_R$, where z_R is the Rayleigh range. The integers l and p are indices characterizing the LG mode. It has been shown [8] that $l\hbar$ represents the orbital angular momentum of each quantum in the mode. Finally, in Eq. (7) \mathcal{E}_{k00} corresponds to the plane-wave ampli-

tude for an axial wave vector k . The plane-wave amplitude and phase emerge directly from Eqs. (7) and (8) by setting $l=0$, $p=0$, and $z_R \rightarrow \infty$.

We now transform to an interaction picture with respect to the unperturbed field Hamiltonian $\hbar\omega a^\dagger a$. The field annihilation and creation operators then acquire the time dependences

$$a(t) = e^{i\omega a^\dagger a t} a e^{-i\omega a^\dagger a t} = a e^{-i\omega t}, \quad (9)$$

$$a^\dagger(t) = e^{i\omega a^\dagger a t} a^\dagger e^{-i\omega a^\dagger a t} = a^\dagger e^{i\omega t}. \quad (10)$$

In the classical limit in which the field forms a coherent beam, we may replace the field operators by c numbers

$$a(t) \rightarrow \alpha e^{-i\omega t}, \quad (11)$$

$$a^\dagger(t) \rightarrow \alpha^* e^{i\omega t}. \quad (12)$$

The coupling between the atom and field may then be written as

$$H_{\text{int}} = -\mathbf{d} \cdot \mathbf{E}(\mathbf{R}) = -i\hbar[\tilde{\pi}^\dagger \alpha f(\mathbf{R}) - \text{H.c.}], \quad (13)$$

where in writing Eq. (13) we have made use of the rotating-wave approximation and have defined

$$\tilde{\pi} = \pi e^{i\omega t}, \quad (14)$$

$$f(\mathbf{R}) = (\mathbf{D}_{12} \cdot \hat{\boldsymbol{\epsilon}}) \mathcal{E}(\mathbf{R}) e^{i\Theta(\mathbf{R})/\hbar}. \quad (15)$$

For convenience, we have not explicitly shown the LG labels klp associated with $\mathcal{E}_{klp}(\mathbf{R})$ and $\Theta_{klp}(\mathbf{R})$ by virtue of Eqs. (7) and (8). In the rest of this section we continue to use this simple notation but resort to the full notation subsequently.

To derive the optical Bloch equations for the atomic density-matrix elements we make the assumption that the position and momentum operators \mathbf{R} and \mathbf{P} may be replaced by their expectation values \mathbf{R}_0 and \mathbf{P}_0 , respectively. This approximation allows the gross motion of the atom to be treated classically, while maintaining a quantum treatment for the internal dynamics of the atom. The validity of the semiclassical approximation requires that the spatial extent of the atomic wave packet be much smaller than the wavelength of the radiation field and that the uncertainty in the Doppler shift be much smaller than the upper-state linewidth of the atom. This is the case for most atoms [1] if the recoil energy of the atom is much smaller than the upper-state linewidth.

Within the semiclassical approximation, the atomic density matrix can be written as

$$\rho = \delta(\mathbf{R} - \mathbf{R}_0) \delta(\mathbf{P} - \mathbf{P}_0) \rho(t), \quad (16)$$

where the internal dynamics of the atom are now contained in $\rho(t)$. The evolution of $\rho(t)$ is given by the well-known relation

$$\frac{d\rho}{dt} = -\frac{i}{\hbar} [H, \rho] + \mathcal{R}\rho, \quad (17)$$

where $\mathcal{R}\rho$ accounts for the relaxation dynamics of the atomic system. By substitution of H and use of the coupling given in

Eq. (13), we obtain the following optical Bloch equations for the atomic density-matrix elements:

$$\frac{d\rho_{22}}{dt} = -2\Gamma\rho_{22} - \alpha f(\mathbf{R}_0)\tilde{\rho}_{12} - \alpha^* f^*(\mathbf{R}_0)\tilde{\rho}_{21}, \quad (18)$$

$$\frac{d\tilde{\rho}_{21}}{dt} = -(\Gamma - i\Delta_0)\tilde{\rho}_{21} + \alpha f(\mathbf{R}_0)(\rho_{22} - \rho_{11}), \quad (19)$$

where $\Delta_0 = \omega - \omega_0$ is the detuning of the field frequency from atomic resonance and $\tilde{\rho}_{21} = \langle \tilde{\pi} \rangle$.

The average radiation force acting on the atom is defined as the average rate of change of the atomic momentum. We may write

$$\langle \mathbf{F} \rangle = -\langle \nabla H_{\text{int}} \rangle. \quad (20)$$

Substitution of Eq. (13) into Eq. (20) and use of Eq. (15) allows the force to be written as $\langle \mathbf{F} \rangle = \langle \mathbf{F}_{\text{diss}} \rangle + \langle \mathbf{F}_{\text{dipole}} \rangle$. Here $\langle \mathbf{F}_{\text{diss}} \rangle$ is the dissipative force given by

$$\langle \mathbf{F}_{\text{diss}} \rangle = -\hbar \nabla \Theta(\mathbf{R}_0) \{ \tilde{\rho}_{12}(t) \alpha f(\mathbf{R}_0) + \tilde{\rho}_{21}(t) \alpha^* f^*(\mathbf{R}_0) \} \quad (21)$$

and $\langle \mathbf{F}_{\text{dipole}} \rangle$ is the dipole force given by

$$\langle \mathbf{F}_{\text{dipole}} \rangle = i\hbar \frac{\nabla \Omega(\mathbf{R}_0)}{\Omega(\mathbf{R}_0)} \{ \tilde{\rho}_{12}(t) \alpha f(\mathbf{R}_0) - \tilde{\rho}_{21}(t) \alpha^* f^*(\mathbf{R}_0) \}, \quad (22)$$

where we have introduced a position-dependent Rabi frequency as $\Omega(\mathbf{R}_0) = |\alpha(\mathbf{D}_{12} \cdot \hat{\mathbf{e}}) \mathcal{E}(\mathbf{R}_0)| / \hbar$.

In the adiabatic approximation [15], the atomic velocity $\mathbf{V} = \mathbf{P}_0 / M$ is assumed to be constant during the time taken for the dipole moment to relax to its steady-state value. The position \mathbf{R}_0 of the atom at time t is then given by

$$\mathbf{R}_0 = \mathbf{r}_0 + \mathbf{V}t, \quad (23)$$

where \mathbf{r}_0 is the (initial) position of the atom when the beam was switched on. Thus we can write

$$f(\mathbf{R}_0) = f(\mathbf{r}_0 + \mathbf{V}t) \quad (24)$$

$$\approx f(\mathbf{r}_0) e^{i\nabla \Theta(\mathbf{r}_0) \cdot \mathbf{V}t}, \quad (25)$$

where we have assumed that the change in the field amplitude is negligible during the time taken for the dipole moment to relax to its steady-state value.

Within the adiabatic approximation, the optical Bloch equations take the form

$$\frac{d\rho_{22}}{dt} = -2\Gamma\rho_{22} - \alpha f(\mathbf{r}_0)\hat{\rho}_{12} - \alpha^* f^*(\mathbf{r}_0)\rho_{22}, \quad (26)$$

$$\frac{d\hat{\rho}_{21}}{dt} = -[\Gamma - i\Delta(\mathbf{r}_0, \mathbf{V})]\hat{\rho}_{21} + \alpha f(\mathbf{r}_0)(\rho_{22} - \rho_{11}), \quad (27)$$

where the total detuning $\Delta(\mathbf{r}_0, \mathbf{V}) = \Delta_0 - \nabla \Theta(\mathbf{r}_0) \cdot \mathbf{V}$ and $\hat{\rho}_{21} = \tilde{\rho}_{21} e^{-i\mathbf{r}_0 \cdot \nabla \Theta(\mathbf{r}_0)}$. The forces can now be written as

$$\langle \mathbf{F}_{\text{diss}} \rangle = -\hbar \nabla \Theta(\mathbf{r}_0) \{ \hat{\rho}_{12}(t) \alpha f(\mathbf{r}_0) + \hat{\rho}_{21} \alpha^* f^*(\mathbf{r}_0) \}, \quad (28)$$

$$\langle \mathbf{F}_{\text{dipole}} \rangle = i\hbar \frac{\nabla \Omega(\mathbf{r}_0)}{\Omega(\mathbf{r}_0)} \{ \hat{\rho}_{12}(t) \alpha f(\mathbf{r}_0) - \hat{\rho}_{21}(t) \alpha^* f^*(\mathbf{r}_0) \}. \quad (29)$$

For given initial conditions the solution of the optical Bloch equations (26) and (27) leads formally to the determination of the forces by direct substitution in Eqs. (28) and (29).

A. Steady state

The steady state occurs when all time derivatives in the optical Bloch equations are set equal to zero and corresponds to the long-time limit. It is not difficult to show that the steady-state solutions to the optical Bloch equations (26) and (27) yield the following expressions for the steady-state forces:

$$\langle \mathbf{F} \rangle = \langle \mathbf{F}_{\text{diss}} \rangle + \langle \mathbf{F}_{\text{dipole}} \rangle, \quad (30)$$

where

$$\langle \mathbf{F}_{\text{diss}}(\mathbf{R}, \mathbf{V}) \rangle = 2\hbar \Gamma \Omega^2(\mathbf{R}) \left(\frac{\nabla \Theta(\mathbf{R})}{\Delta^2(\mathbf{R}, \mathbf{V}) + 2\Omega^2(\mathbf{R}) + \Gamma^2} \right), \quad (31)$$

$$\langle \mathbf{F}_{\text{dipole}}(\mathbf{R}, \mathbf{V}) \rangle = -2\hbar \Omega(\mathbf{R}) \nabla \Omega(\mathbf{R}) \times \left(\frac{\Delta(\mathbf{R}, \mathbf{V})}{\Delta^2(\mathbf{R}, \mathbf{V}) + 2\Omega^2(\mathbf{R}) + \Gamma^2} \right), \quad (32)$$

where we have redefined the notation such that \mathbf{R} now stands for the position of the atom (instead of \mathbf{r}_0). The above results are the same as those presented in our previous work where perturbation techniques for time-dependent Heisenberg operators have been used [11]. The dependence on the decay constant and on saturation are in agreement with our earlier heuristic approach.

B. Transients

Torrey [16] gave detailed solutions of the original optical Bloch equations. He also recognized that there were three special cases of interest that have relatively simple solutions. These were for strong collisions when the natural lifetime of the state may be replaced by the collision shortened lifetime, exact resonance and for intense external fields. His approach was applied by Allen and Eberly [17] to the optical Bloch equations. Consequently, in a similar way, the evolution of the forces from the instant the light beam is switched on can also be examined for a number of special cases. In fact, radiation effects have been examined in detail for atoms excited by plane-wave light [18]; the cases considered were (i) an atom with all relaxation constants equal to zero, (ii) a weak beam, (iii) exact resonance, and (iv) steady state achieved by an intense field. This treatment may be readily generalized for Laguerre-Gaussian light.

We shall settle simply for the steady-state case already considered in Sec. II A because the general time dependence of the density-matrix elements can be determined more readily for arbitrary parameter values by the numerical solution of the optical Bloch equations (26) and (27). This enables the evolution of the corresponding forces to be displayed. We display the results for a Laguerre-Gaussian mode

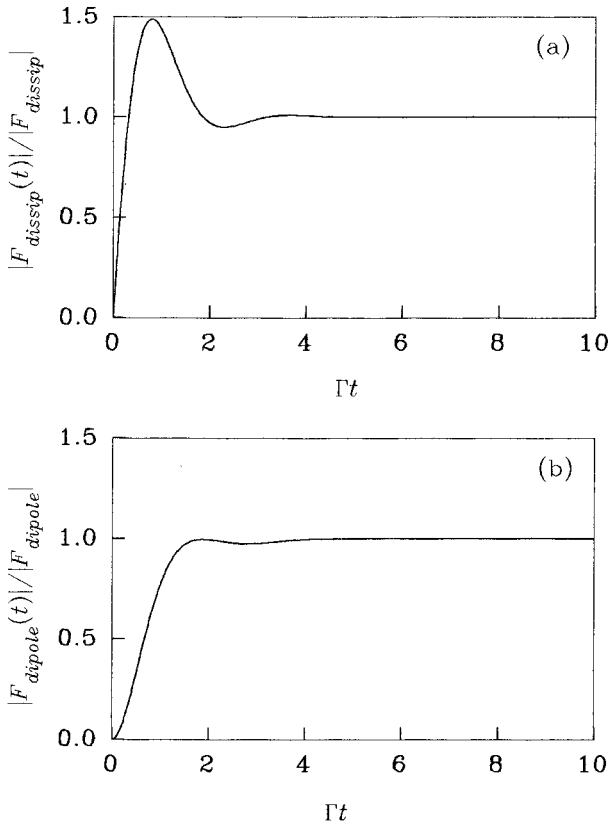


FIG. 1. Variation with time (in units of Γ^{-1}) of (a) the average dissipative force and (b) the average dipole force in units of the corresponding steady-state values for a stationary atom in a single LG beam. [The time variation of the corresponding torque would be the same as in (a), but in units of the steady-state torque.] See the text for the values assumed for the parameters.

with $l=1$ and $p=0$ such that $\Omega(\mathbf{r}_0)=\Gamma$; $\Delta=-\Gamma$ and $\omega(0)=35\lambda$, where $\lambda=280$ nm is the atomic transition wavelength. The results shown in Figs. 1(a) and 1(b) depict the evolutions of the dissipative and dipole forces [given by Eqs. (28) and (29), respectively]. These figures show clearly that the dipole moment, and hence force components, relax to their steady-state values within a time of the order of Γ^{-1} .

III. STEADY-STATE DYNAMICS

A. Single LG beam

From the results of the preceding section it is clear that, for elapsed times greater than the inverse relaxation parameters, the total force on a two-level atom has a steady-state value, exhibits position dependence, and is naturally divisible into two terms. Restoring the explicit reference to a specific Laguerre-Gaussian mode, the steady-state force on a moving atom due to a single Laguerre-Gaussian beam propagating along the positive z axis is written

$$\langle \mathbf{F} \rangle_{klp} = \langle \mathbf{F}_{\text{diss}} \rangle_{klp} + \langle \mathbf{F}_{\text{dipole}} \rangle_{klp}, \quad (33)$$

where

$$\begin{aligned} \langle \mathbf{F}_{\text{diss}}(\mathbf{R}, \mathbf{V}) \rangle_{klp} \\ = 2\hbar\Gamma\Omega_{klp}^2(\mathbf{R}) \left(\frac{\nabla\Theta_{klp}(\mathbf{R})}{\Delta_{klp}^2(\mathbf{R}, \mathbf{V}) + 2\Omega_{klp}^2(\mathbf{R}) + \Gamma^2} \right) \end{aligned} \quad (34)$$

and

$$\begin{aligned} \langle \mathbf{F}_{\text{dipole}}(\mathbf{R}, \mathbf{V}) \rangle_{klp} \\ = -2\hbar\Omega_{klp}(\mathbf{R})\nabla\Omega_{klp} \left(\frac{\Delta_{klp}(\mathbf{R}, \mathbf{V})}{\Delta_{klp}^2(\mathbf{R}, \mathbf{V}) + 2\Omega_{klp}^2(\mathbf{R}) + \Gamma^2} \right), \end{aligned} \quad (35)$$

where $\mathbf{R}(t)$ now denotes the current position vector of the atom and $\mathbf{V}=\dot{\mathbf{R}}$. The effective detuning $\Delta_{klp}(\mathbf{R}, \mathbf{V})$ is now both position and velocity dependent

$$\Delta_{klp}(\mathbf{R}, \mathbf{V}) = \Delta_0 - \mathbf{V} \cdot \nabla\Theta_{klp}(\mathbf{R}, \mathbf{V}). \quad (36)$$

The dissipative force, proportional to the phase gradient, is given by Eq. (34). This force can be visualized as arising locally from the absorption followed by spontaneous emission of light by the atom. The dipole force, which is proportional to the gradient of the field intensity, subsumed in the position-dependent Rabi frequency, is given by Eq. (35). Both forces play important roles in the cooling and trapping of the atom. The dissipative component is responsible for the existence of a frictional force in a configuration involving two counterpropagating waves, while the dipole force confines the atom to the high-intensity regions of the field when the detuning is below resonance [7].

B. Low-velocity limit

In order to elucidate the nature of the interaction between the LG beam and the atom we consider the low-velocity limit of the dissipative and dipole forces. However, in the computational evaluation of the full extent of the interaction to study the dynamics of the atom described later in this paper, this approximation will not be made. The assumption involved in the low-velocity limit is that the Doppler shift induced by the motion of the atom is smaller than the atomic width $\mathbf{V} \cdot \nabla\Theta \ll \Gamma$. In this case we may expand the denominators of Eqs. (34) and (35) retaining terms up to those linear in the velocity. We can thus write each force as the sum of a static (velocity-independent) and dynamic (velocity-dependent) components. The static components are given by

$$\begin{aligned} \langle \mathbf{F}_{\text{diss}}^0(\mathbf{R}) \rangle_{klp} = \frac{2\hbar\Gamma\Omega_{klp}^2(\mathbf{R})}{\Delta_0^2 + 2\Omega_{klp}^2(\mathbf{R}) + \Gamma^2} \left[\{ \eta_{klp}(\mathbf{R}) + k \} \hat{\mathbf{z}} + \frac{l}{r} \hat{\phi} \right. \\ \left. + \xi_k(\mathbf{R}) \hat{\mathbf{r}} \right], \end{aligned} \quad (37)$$

$$\langle \mathbf{F}_{\text{react}}^0(\mathbf{R}) \rangle_{klp} = - \frac{2\hbar\Delta_0\Omega_{klp}(\mathbf{R})\nabla\Omega_{klp}(\mathbf{R})}{\Delta_0^2 + 2\Omega_{klp}^2(\mathbf{R}) + \Gamma^2} \quad (38)$$

and the dynamic components by

$$\begin{aligned} \langle \mathbf{F}_{\text{diss}}^V(\mathbf{R}, \mathbf{V}) \rangle &= \frac{4\hbar\Gamma\Delta_0\Omega_{klp}^2(\mathbf{R})}{[\Delta_0^2 + 2\Omega_{klp}^2(\mathbf{R}) + \Gamma^2]^2} \left[\{ \eta_{klp}(\mathbf{R}) + k \} \hat{\mathbf{z}} \right. \\ &\quad + \frac{l}{r} \hat{\phi} + \xi_k(\mathbf{R}) \hat{\mathbf{r}} \left. \right] \left[\{ \eta_{klp}(\mathbf{R}) + k \} V_z + \frac{l}{r} V_\phi \right. \\ &\quad \left. + \xi_k(\mathbf{R}) V_r \right], \end{aligned} \quad (39)$$

$$\begin{aligned} \langle \mathbf{F}_{\text{dipole}}^V(\mathbf{R}, \mathbf{V}) \rangle &= \frac{2\hbar\Omega_{klp}(\mathbf{R})\nabla\Omega(\mathbf{R})}{[\Delta_0^2 + 2\Omega_{klp}^2(\mathbf{R}) + \Gamma^2]} \\ &\quad \times \left(1 - \frac{2\Delta_0^2}{[\Delta_0^2 + 2\Omega_{klp}^2(\mathbf{R}) + \Gamma^2]} \right) \\ &\quad \times \left[\{ \eta_{klp}(\mathbf{R}) + k \} V_z + \frac{l}{r} V_\phi + \xi_k(\mathbf{R}) V_r \right]. \end{aligned} \quad (40)$$

In the equations above V_z , V_ϕ , and V_r are, respectively, the axial, azimuthal, and radial components of the velocity and the functions $\eta_{klp}(\mathbf{R})$ and $\xi_k(\mathbf{R})$ are defined by

$$\eta_{\pm klp} = \pm \frac{kr^2}{2(z^2 + z_R^2)} \left[1 - \frac{2z^2}{z^2 + z_R^2} \right] \pm (2p \pm l + 1) \frac{z_R}{z^2 + z_R^2}, \quad (41)$$

$$\xi_{\pm k}(\mathbf{R}) = \pm \frac{krz}{z^2 + z_R^2}. \quad (42)$$

We make the additional assumption that the atom moves in a region of the beam for which $z \ll z_R$ and we can then ignore the z dependence in $\Omega_{klp}(\mathbf{R})$ and set $\eta_{klp}(\mathbf{R})=0$ and $\xi_k(\mathbf{R})=0$. We may also write to a good approximation

$$\begin{aligned} \nabla\Omega_{klp}(\mathbf{R}) &\approx \left\{ \left[\frac{|l|}{r} - \frac{2r}{w_0^2} \right] \Omega_{klp}(\mathbf{R}) \right. \\ &\quad \left. - \frac{2\sqrt{2p}}{w_0} \Omega_{k|l|+1p-1}(\mathbf{R}) \right\} \hat{\mathbf{r}}. \end{aligned} \quad (43)$$

In the low-velocity limit with $z \ll z_R$, the static dissipative and dipole forces become

$$\langle \mathbf{F}_{\text{diss}}^0(\mathbf{R}) \rangle_{klp} \approx \frac{2\hbar\Gamma\Omega_{klp}^2(\mathbf{R})}{\Delta_0^2 + 2\Omega_{klp}^2(\mathbf{R}) + \Gamma^2} \left[k\hat{\mathbf{z}} + \frac{l}{r} \hat{\phi} \right], \quad (44)$$

$$\begin{aligned} \langle \mathbf{F}_{\text{dipole}}^0(\mathbf{R}) \rangle_{klp} &\approx - \frac{2\hbar\Delta_0\Omega_{klp}(\mathbf{R})}{\Delta_0^2 + 2\Omega_{klp}^2(\mathbf{R}) + \Gamma^2} \left(\left[\frac{|l|}{r} - \frac{2r}{w_0^2} \right] \Omega_{klp}(\mathbf{R}) \right. \\ &\quad \left. - \frac{2\sqrt{2p}}{w_0} \Omega_{k|l|+1p-1}(\mathbf{R}) \right) \hat{\mathbf{r}}, \end{aligned} \quad (45)$$

while the dynamic dissipative and dipole forces become

$$\langle \mathbf{F}_{\text{diss}}^V(\mathbf{R}, \mathbf{V}) \rangle \approx \frac{4\hbar\Gamma\Delta_0\Omega_{klp}^2(\mathbf{R})}{[\Delta_0^2 + 2\Omega_{klp}^2(\mathbf{R}) + \Gamma^2]^2} \left[\left\{ k^2 V_z + \frac{kl}{r} V_\phi \right\} \hat{\mathbf{z}} \right. \\ \left. + \frac{kl}{r} V_z \hat{\phi} \right], \quad (46)$$

$$\begin{aligned} \langle \mathbf{F}_{\text{dipole}}^V(\mathbf{R}, \mathbf{V}) \rangle &\approx \frac{2\hbar\Omega_{klp}(\mathbf{R})}{[\Delta_0^2 + 2\Omega_{klp}^2(\mathbf{R}) + \Gamma^2]^2} \\ &\quad \times \left(1 - \frac{2\Delta_0^2}{[\Delta_0^2 + 2\Omega_{klp}^2(\mathbf{R}) + \Gamma^2]} \right) \\ &\quad \times \left[kV_z + \frac{l}{r} V_\phi \right] \left(\left[\frac{|l|}{r} - \frac{2r}{w_0^2} \right] \Omega_{klp}(\mathbf{R}) \right. \\ &\quad \left. - \frac{2\sqrt{2p}}{w_0} \Omega_{k|l|+1p-1}(\mathbf{R}) \right) \hat{\mathbf{r}}. \end{aligned} \quad (47)$$

Equations (44) and (46) show that the dissipative force has static components in both the axial and azimuthal directions; the latter is equivalent to a torque about the beam axis. These forces combine with dynamic components in the axial and azimuthal directions. Note that within this approximation, Eq. (46) shows that there is a reciprocal relationship between the axial and azimuthal motions. An atom moving initially in the z direction will induce a force in the azimuthal direction and vice versa. It may be seen from Eqs. (45) and (47) that the dipole force consists of static and dynamic components, both of which are in the radial direction.

The static component of the dipole force, given by Eq. (38), attracts the atom to the high-intensity regions of the field when the detuning is below resonance. This force can be derived from a potential [7]

$$\langle U(\mathbf{R}) \rangle_{klp} = \frac{\hbar\Delta_0}{2} \ln \left[1 + \frac{2\Omega_{klp}^2(\mathbf{R})}{\Delta_0^2 + \Gamma^2} \right] \quad (48)$$

such that $\langle \mathbf{F}_{klp}^0 \rangle = -\nabla \langle U(\mathbf{R}) \rangle_{klp}$. This potential exhibits minima in the high-intensity regions of the beam for an atom tuned below resonance where $\Delta_0 < 0$. For $\Delta_0 > 0$, we have trapping in the low-intensity (dark) regions of the field. As an illustration, we consider the LG mode for which $l=1$, $p=0$. The potential is

$$\langle U \rangle_{k10} = \frac{\hbar\Delta_0}{2} \ln \left[1 + \frac{2\Omega_{k10}^2(\mathbf{R})}{\Delta_0^2 + \Gamma^2} \right]. \quad (49)$$

At the beam waist $z=0$, the minimum occurs at $r=r_0$ where

$$r_0 = w_0/\sqrt{2}. \quad (50)$$

For a beam propagating along the z axis it is easy to verify that the locus of the potential minimum in the xy plane is a circle given by

$$x^2 + y^2 = r_0^2. \quad (51)$$

Expanding the potential in powers of $(r-r_0)$ we have the parabolic approximation

$$\langle U \rangle_{k10} \approx U_0 + \frac{1}{2} \Lambda_{k10} (r-r_0)^2, \quad (52)$$

where U_0 is the potential depth given by

$$U_0 = \frac{1}{2} \hbar \Delta_0 \ln \left[1 + \frac{2\Omega_{k10}^2(r_0)}{\Delta_0^2 + \Gamma^2} \right] \quad (53)$$

and Λ_{k10} is an effective elastic constant given by

$$\Lambda_{k10} = \frac{4\hbar|\Delta_0|}{\Delta_0^2 + 2e^{-1}\Omega_{k00}^2 + \Gamma^2} \left(\frac{e^{-1}\Omega_{k00}^2}{w_0^2} \right). \quad (54)$$

The atom is considered trapped if its kinetic energy is less than U_0 and will exhibit quasiharmonic vibrational motion about $r=r_0$. The characteristic angular frequency is equal to $\sqrt{\Lambda_{k10}/M}$, where M is the atomic mass.

C. Counterpropagating LG beams

1. One-dimensional case

We have seen above that an atom immersed in a Laguerre-Gaussian beam will experience a dissipative force that is predominantly in the direction of propagation and a dipole force in the radial direction. If a second beam is added propagating in the opposite direction, we have a configuration that can be referred to as the one-dimensional (1D) counterpropagating beam configuration. In this paper the beams are assumed to be independent of each other in that their phases are not locked. The case in which the beams are phase locked to form a standing wave will be considered elsewhere. For independent counterpropagating LG beams we can write the mean force on the atom as a sum of forces due to individual beams

$$\begin{aligned} \langle \mathbf{F}_{\text{diss}} \rangle_{kl_1p_1, -kl_2p_2} &= 2\hbar\Gamma\Omega_{klp}^2(\mathbf{R}) \\ &\times \left[\frac{\nabla\Theta_{kl_1p_1}(\mathbf{R})}{\Delta_{kl_1p_1}^2(\mathbf{R}, \mathbf{V}) + 2\Omega_{kl_1p_1}^2(\mathbf{R}) + \Gamma^2} \right. \\ &\left. + \frac{\nabla\Theta_{-kl_2p_2}(\mathbf{R})}{\Delta_{-kl_2p_2}^2(\mathbf{R}, \mathbf{V}) + 2\Omega_{-kl_2p_2}^2(\mathbf{R}) + \Gamma^2} \right], \end{aligned} \quad (55)$$

$$\begin{aligned} \langle \mathbf{F}_{\text{dipole}} \rangle_{kl_1p_1, -kl_2p_2} &= -2\hbar\Omega_{klp}(\mathbf{R})\nabla\Omega_{klp} \\ &\times \left[\frac{\Delta_{kl_1p_1}(\mathbf{R}, \mathbf{V})}{\Delta_{kl_1p_1}^2(\mathbf{R}, \mathbf{V}) + 2\Omega_{kl_1p_1}^2(\mathbf{R}) + \Gamma^2} \right. \\ &\left. + \frac{\Delta_{-kl_2p_2}(\mathbf{R}, \mathbf{V})}{\Delta_{-kl_2p_2}^2(\mathbf{R}, \mathbf{V}) + 2\Omega_{-kl_2p_2}^2(\mathbf{R}) + \Gamma^2} \right], \end{aligned} \quad (56)$$

where we have assumed that $p_1=p_2=p$ and either $(l_1=-l_2=l)$ or $(l_1=l_2=l)$.

In the low-velocity regime, for an atom close to the beam waist, we may make use of Eqs. (44)–(47). The total static dissipative and dipole forces are then given by

$$\langle \mathbf{F}_{\text{diss}}^0(\mathbf{R}) \rangle_{kl_1p_1, -kl_2p_2} \approx \frac{2\hbar\Gamma\Omega_{klp}^2(\mathbf{R})}{\Delta_0^2 + 2\Omega_{klp}^2(\mathbf{R}) + \Gamma^2} \left[\frac{l_1}{r} + \frac{l_2}{r} \right] \hat{\phi}, \quad (57)$$

$$\begin{aligned} \langle \mathbf{F}_{\text{dipole}}^0(\mathbf{R}) \rangle_{kl_1p_1, -kl_2p_2} &\approx -\frac{4\hbar\Delta_0\Omega_{klp}(\mathbf{R})}{\Delta_0^2 + 2\Omega_{klp}^2(\mathbf{R}) + \Gamma^2} \\ &\times \left(\left[\frac{|l|}{r} - \frac{2r}{w_0^2} \right] \Omega_{klp}(\mathbf{R}) \right. \\ &\left. - \frac{2\sqrt{2p}}{w_0} \Omega_{k|l|+1, p-1}(\mathbf{R}) \right) \hat{\mathbf{r}} \end{aligned} \quad (58)$$

and the total dynamic dissipative and dipole forces are

$$\begin{aligned} \langle \mathbf{F}_{\text{diss}}^V(\mathbf{R}, \mathbf{V}) \rangle_{kl_1p_1, -kl_2p_2} &\approx \frac{4\hbar\Gamma\Delta_0\Omega_{klp}^2(\mathbf{R})}{[\Delta_0^2 + 2\Omega_{klp}^2(\mathbf{R}) + \Gamma^2]^2} \\ &\times \left[\left\{ 2k^2V_z + \frac{k}{r}(l_1 - l_2)V_\phi \right\} \right. \\ &\left. \times \hat{\mathbf{z}} + \frac{k}{r}(l_1 - l_2)V_z\hat{\phi} \right], \end{aligned} \quad (59)$$

$$\begin{aligned} \langle \mathbf{F}_{\text{dipole}}^V(\mathbf{R}, \mathbf{V}) \rangle_{kl_1p_1, -kl_2p_2} &\approx \frac{2\hbar\Omega_{klp}(\mathbf{R})}{[\Delta_0^2 + 2\Omega_{klp}^2(\mathbf{R}) + \Gamma^2]} \\ &\times \left(1 - \frac{2\Delta_0^2}{[\Delta_0^2 + 2\Omega_{klp}^2(\mathbf{R}) + \Gamma^2]} \right) \\ &\times \left(\left[\frac{|l|}{r} - \frac{2r}{w_0^2} \right] \Omega_{klp}(\mathbf{R}) \right. \\ &\left. - \frac{2\sqrt{2p}}{w_0} \Omega_{k|l|+1, p-1}(\mathbf{R}) \right) \\ &\times (l_1 + l_2) \frac{V_\phi}{r} \hat{\mathbf{r}}. \end{aligned} \quad (60)$$

From Eq. (58) we see that the velocity-independent dipole force is simply double that of a single-beam case. The dissipative force, however, depends on the relative signs of l_1 and l_2 . For $l_1=l_2=l$ we have

$$\langle \mathbf{F}_{\text{dipole}}^0(\mathbf{R}) \rangle_{klp, -klp} \approx \frac{4\hbar\Gamma\Omega_{klp}^2(\mathbf{R})}{\Delta_0^2 + 2\Omega_{klp}^2(\mathbf{R}) + \Gamma^2} \left(\frac{l}{r} \right) \hat{\phi}, \quad (61)$$

$$\langle \mathbf{F}_{\text{diss}}^V(\mathbf{R}, \mathbf{V}) \rangle_{klp, -klp} \approx \frac{8\hbar\Gamma\Delta_0\Omega_{klp}^2(\mathbf{R})}{[\Delta_0^2 + 2\Omega_{klp}^2(\mathbf{R}) + \Gamma^2]^2} k^2V_z\hat{\mathbf{z}}. \quad (62)$$

Thus, for $l_1=l_2=l$ we have a torque about the beam axis and an axial cooling or heating force, depending on the sign of Δ_0 .

For the case $l_1=-l_2=l$, we have

$$\langle \mathbf{F}_{\text{diss}}^0(\mathbf{R}) \rangle_{klp, -k-lp} = 0, \quad (63)$$

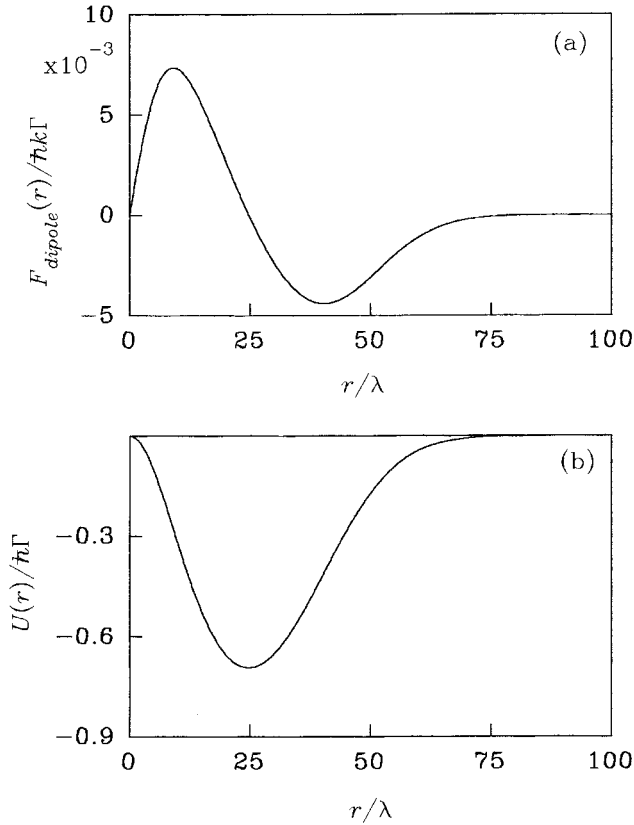


FIG. 2. (a) Radial distribution of the dipole force due to 1D counterpropagating Laguerre-Gaussian beams at $z=0$. Here $l_1=-l_2=1$, $p_1=p_2=0$, and the parameters are $\Delta_0=-\Gamma$, $\Omega_{k00}=1.648\Gamma$, and $\omega_0=35\lambda$. (b) Radial potential distribution corresponding to (a).

$$\begin{aligned} \langle \mathbf{F}_{\text{diss}}^V(\mathbf{R}, \mathbf{V}) \rangle_{klp-k-lp} &\approx \frac{8\hbar\Gamma\Delta_0\Omega_{klp}^2(\mathbf{R})}{[\Delta_0^2 + 2\Omega_{klp}^2(\mathbf{R}) + \Gamma^2]^2} \\ &\times \left\{ \left[k^2 V_z + \frac{kl}{r} V_\phi \right] \hat{\mathbf{z}} + \frac{kl}{r} V_z \hat{\phi} \right\}. \end{aligned} \quad (64)$$

The static force in this case is zero, while the velocity-dependent force contains extra terms that arise from the orbital angular momentum of the counterpropagating Laguerre-Gaussian beams. As with the one-beam case, we again see force components arising from the reciprocating interchange between the axial and azimuthal motions.

2. Two-dimensional, three-dimensional, and three coplanar beams

The 2D case arises when a second pair of counterpropagating LG beams is arranged orthogonal to the first pair. The total force can again be written as a sum of forces from each of the beams. However, in addition to the reciprocal action between the azimuthal and axial motions in each pair of beams, there is also the fact that the azimuthal atomic motion associated with one beam is part of the axial motion in the other. In other words, there is an additional level of reciprocity between the components of the motion arising from the presence of two pairs of counterpropagating beams.

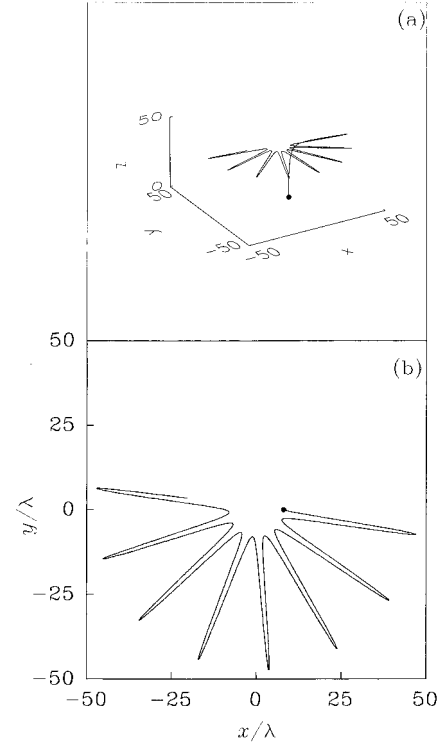


FIG. 3. (a) Trajectory of a Mg^+ ion in 1D counterpropagating LG beams for $l_1=-l_2=1$ and $p_1=p_2=0$. All distances are in units of the wavelength of the light λ . The initial position is $\mathbf{R}_0=8\lambda\hat{\mathbf{x}}$ and the initial velocity components are $V_z=5.0\text{ ms}^{-1}$ and $V_r=0=V_\phi$. (b) Projection in the xy plane of the ion trajectory shown in (a). In this and subsequent figures, the initial position is indicated by a full circle. See the text for the values assumed for the other parameters.

There are also two overlapping dipole potential distributions arising from the orthogonal beams. It is easy to see for beam pairs for which $l_1=-l_2=1$ and $p_1=p_2=0$ and where the axes are such that one pair is along the z axis and the second along the x axis, the potential minima are four times as deep as that of a single beam. The minima are situated at the space points defined by the two equations

$$x^2 + y^2 = w_0^2/2, \quad (65)$$

$$y^2 + z^2 = w_0^2/2. \quad (66)$$

These equations apply the additional constraint $x = \pm z$. Atoms subject to such 2D counterpropagating beams will congregate at points lying on the curve defined by two intersecting circles, one on the plane $x+z=0$ and the other on the plane $x-z=0$.

When a third set of beams is arranged orthogonal to the other two orthogonal pairs we have 3D counterpropagating LG beams. The common potential minima in this case occur at eight distinct points defined by

$$x = \pm w_0/\sqrt{2}, \quad y = \pm w_0/\sqrt{2}, \quad z = \pm w_0/\sqrt{2} \quad (67)$$

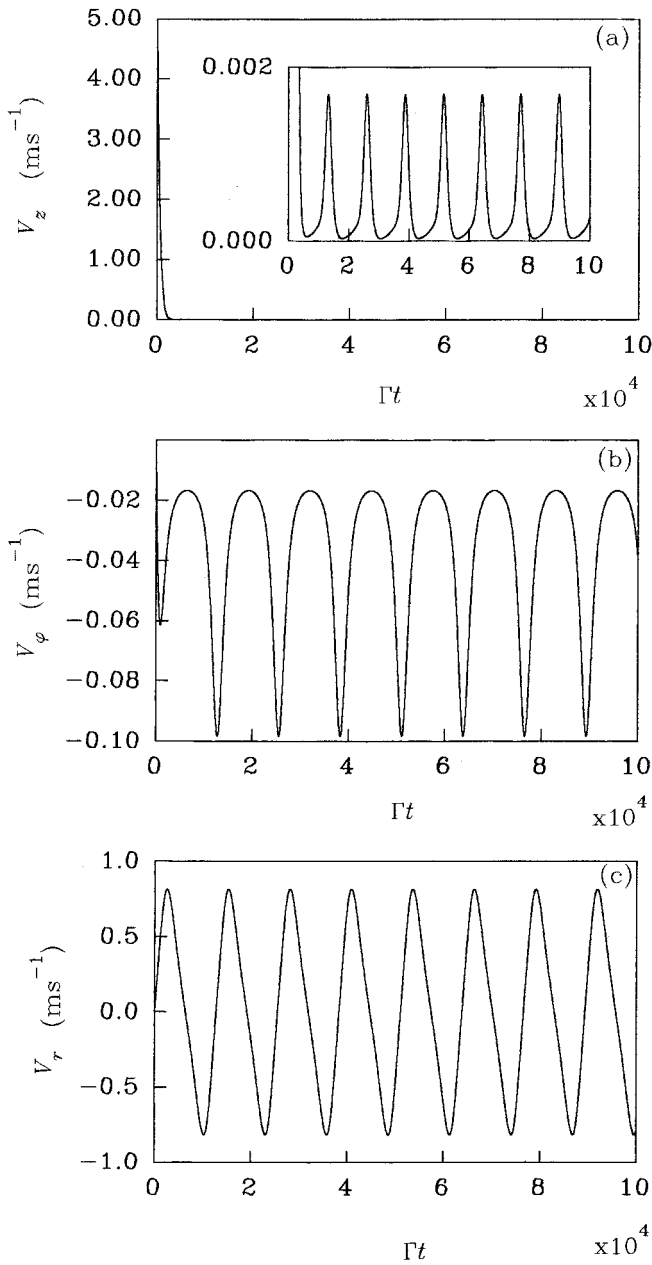


FIG. 4. Variations of the velocity components for the case in Fig. 3. (a) Evolution of V_z indicating axial cooling. The inset to this figure shows small oscillations of V_z due to reciprocating effects. (b) Evolution of V_ϕ and (c) evolution of V_r . Both (b) and (c) indicate the rapid onset of oscillatory motions of the same period.

and are six times as deep as the potential due to one beam. However, in this case the detailed polarization gradients are such as to make further study of this configuration nontrivial.

Finally, we consider the case of three coplanar beams [19] in the x - y plane in a symmetric configuration in which the angle between adjacent beams is $2\pi/3$. This leads to three overlapping circles that meet at two distinct points at

$$x=0, \quad y=0, \quad z=\pm w_0/\sqrt{2} \quad (68)$$

and the potential well is three times as deep as for a single beam.

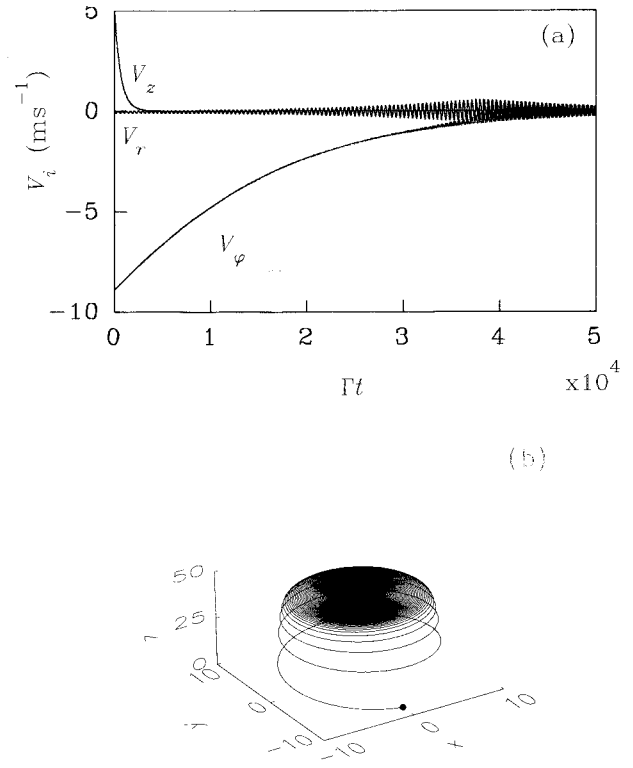


FIG. 5. (a) Evolution of the velocity components of a Mg^+ ion subject to Laguerre-Gaussian 1D counterpropagating beams with $l_1=l_2=1$, $p_1=p_2=0$, and $|\mathbf{B}|=1$ T. Initially the ion possesses both azimuthal and axial velocity components $V_z=5.0$ ms^{-1} and $V_\phi=-8.9$ ms^{-1} . (b) Trajectory of the Mg^+ in (a). All distances are in units of the wavelength of the light λ .

IV. Mg^+ IN MULTIPLE BEAMS

The emphasis throughout this paper is on the physics introduced by the orbital angular momentum aspects of the interaction of atoms with Laguerre-Gaussian light. In the theoretical analysis presented in the preceding section we were able to infer that an atom in a configuration of such beams is subject to axial forces and various forms of static and dynamic rotational forces and that axial and rotational motions influence each other in a rather intricate way. Furthermore, a system of multiple Laguerre-Gaussian beams presents an atom with well-defined potential landscapes that depend on the angular momentum quantum numbers and beam configuration. For example, in the 1D case with a given set of parameters, a given atom should have well-defined quasiharmonic vibrational states associated with the potential profiles.

To illustrate these features we consider the case of Mg^+ in Laguerre-Gaussian light. The Mg^+ mass is $M=4.0\times 10^{-26}$ kg; the transition wavelength is $\lambda=280.1$ nm and its half-width is $\Gamma=2.7\times 10^8$ s^{-1} . To illustrate the theory typical beam parameters are exemplified by the choices $\Delta_0=-\Gamma$, $\Omega_{k00}=1.648\Gamma$, and $w_0=35\lambda$. The equation of motion of a Mg^+ ion in multiple LG beams is written as

$$M \frac{\partial^2 \mathbf{R}(t)}{\partial t^2} = \sum_i \{ \langle \mathbf{F}_{\text{diss}}(\mathbf{R}, \mathbf{V}) \rangle_{k_i, l_i, p_i} + \langle \mathbf{F}_{\text{dipole}}(\mathbf{R}, \mathbf{V}) \rangle_{k_i, l_i, p_i} \} + Q\mathbf{V} \times \mathbf{B}, \quad (69)$$

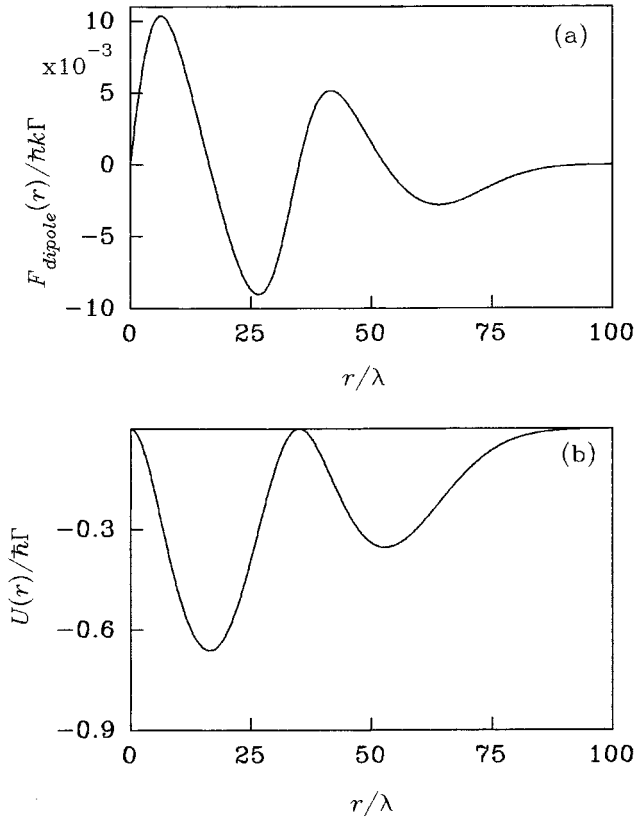


FIG. 6. (a) Radial distribution of the dipole force due to 1D counterpropagating Laguerre-Gaussian beams at $z=0$. Here $l_1=-l_2=1$, $p_1=p_2=1$, and the parameters are $\Delta_0=-\Gamma$, $\Omega_{k00}=1.648\Gamma$, and $\omega_0=35\lambda$. (b) Radial potential distribution corresponding to (a).

where Q is the ionic charge and we have included the last term on the right-hand side to allow for the possibility of an applied external magnetic field. The summation indicates the vector addition over force contributions arising from individual beams. The forces from each beam are taken in their unapproximated forms given by Eqs. (34) and (35).

We begin by considering 1D counterpropagating beams in the absence of the magnetic field. Figure 2(a) displays the dipole force as given by Eq. (56) as a function of radial distance r at $y=0$ and $z=0$. The beam quantum numbers are such that $l_1=-l_2=1$ and $p_1=p_2=0$ and the parameters are $\Delta_0=-\Gamma$, $\Omega_{k00}=1.648\Gamma$, and $w_0=35\lambda$. Figure 2(b) displays the corresponding radial potential distribution. The maximum intensity is located at points where $r=w_0/\sqrt{2}=24.75\lambda$. As expected, we see that for $\Delta_0<0$ the dipole potential exhibits a minimum at points where the intensity is maximum. The vibrational states in the parabolic approximation have an elastic constant that is twice that for the one-beam case as given by Eq. (54). The vibrational frequency corresponding to the above parameters is

$$\nu \approx \frac{1}{2\pi} \left(\frac{8\hbar|\Delta_0|e^{-1}\Omega_{k00}^2}{Mw_0^2[\Delta_0^2+2e^{-1}\Omega_{k00}^2+\Gamma^2]} \right)^{1/2}. \quad (70)$$

For the parameter values specified above this yields $\nu \approx 2.0 \times 10^4 \Gamma$.

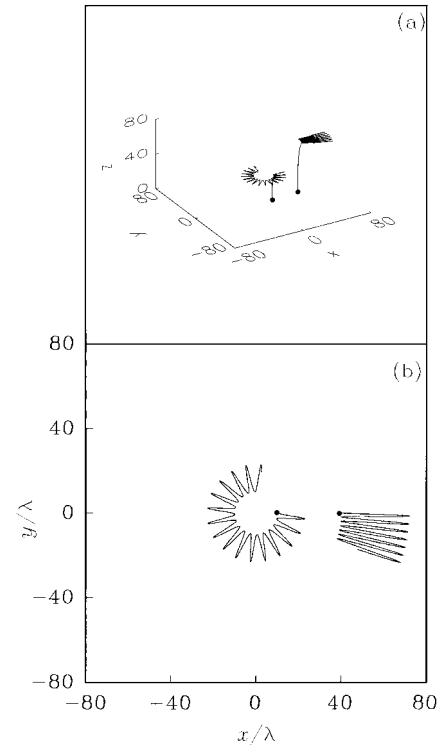


FIG. 7. (a) Trajectories of a Mg^+ ion in 1D counterpropagating LG beams for $l_1=-l_2=1$ and $p_1=p_2=1$ for two different initial positions: one is at $\mathbf{R}_0=10\lambda\hat{\mathbf{x}}$ and the second is at $\mathbf{R}_0=40\lambda\hat{\mathbf{x}}$. All distances are in units of the wavelength of the light λ . The initial velocity components in both cases are $V_z=5.0 \text{ ms}^{-1}$ and $V_r=0=V_\phi$. (b) Projections in the xy plane of the ion trajectories shown in (a). See the text for the assumed values of the other parameters.

Figure 3(a) displays the trajectory of the ion as a function of time and Fig. 3(b) depicts its projection onto the xy plane. The initial position is at $\mathbf{R}_0=8\lambda\hat{\mathbf{x}}$ and the initial velocity components are $V_z=5.0 \text{ ms}^{-1}$, $V_\phi=0=V_r$. It is clear from the figure that the atom, subject to an axial friction force, has been slowed axially. Once the atom is moving sufficiently slowly, it starts a vibrational motion about the radial coordinate $r=w_0/\sqrt{2}$, accompanied by a slow rotational motion. The latter, according to Eq. (46), is attributed to the azimuthal component of the dissipative force induced by the axial motion.

Figure 4 displays the evolution of the velocity components. The axial velocity is seen to decay almost to zero. However, closer inspection, as shown by the inset to Fig. 4(a), reveals that the axial motion exhibits periodic oscillations that are attributable to a reciprocating force arising from the periodic azimuthal motion, depicted in Fig. 4(b). The period associated with these figures is indeed about $2.0 \times 10^4 \Gamma$ as in the estimate based on Eq. (70). An important feature displayed by the results depicted in Figs. 3 and 4 is that changing the sign of the angular momentum quantum number l from $+1$ to -1 , which is readily achievable [8,9], causes the change in the rotational motion from clockwise to the opposite (counterclockwise) sense.

Figure 5 is concerned with the case $l_1=l_2=+1$ and $p_1=p_2=0$ in the presence of a magnetic field $|\mathbf{B}|=1 \text{ T}$ directed along the positive z axis. From Eqs. (61) and (62) we

deduce that, besides the ion cyclotron motion due the magnetic field, the main effects are in the form of an axial friction force provided that $\Delta_0 < 0$ and a static torque about the beam axis that acts upon the ion azimuthally. Figure 5(a) displays the evolution of velocity components for the case $\Delta_0 = -\Gamma$. The initial ion position is $\mathbf{R}(0) = -8\lambda\hat{\mathbf{y}}$ and the initial velocity components are $V_r = 0$, $V_\phi = -8.9 \text{ ms}^{-1}$, and $V_z = 5.0 \text{ ms}^{-1}$. We see that the torque due to the LG beams generates a braking effect on the cyclotron motion, while the axial motion is gradually cooled by the axial friction force. All these features can be inferred from the trajectory shown in Fig. 5(b). If the sign of l in both beams were to be changed, but \mathbf{B} kept in the same direction, we would have heating of the azimuthal motion, while the axial motion would still be cooled. Clearly the former case amounts to a decrease in angular motion due to the LG beam, while the latter is equivalent to the enhancement of the angular motion. These phenomena are attributable only to the angular momentum properties of the LG beams [20].

Figure 6 is concerned with counterpropagating beams with the next-higher-order LG modes $l_1 = -l_2 = 1$ and $p_1 = p_2 = 1$ and no external magnetic field. Other parameter values are $\Omega_{k00} = 1.648$ and $\Delta_0 = -\Gamma$. Figures 3(a) and 3(b) display the radial distribution of the dipole force and corresponding potential, respectively. We now have two potential wells with minima at $r = 0.468w_0 \equiv 16.38\lambda$ and $r = 1.5w_0 \equiv 52.86\lambda$. The ion is destined to oscillate about one of these points, depending on the initial conditions. This can be seen in Fig. 7 for an atom with $V_x = 0 = V_y$ and $V_z = 5.0 \text{ ms}^{-1}$. The inner curve depicts the trajectory when the atom begins at $\mathbf{R}_0 = 10\lambda\hat{\mathbf{x}}$ and the outer curve when it begins $\mathbf{R}_0 = 40\lambda\hat{\mathbf{y}}$.

Figure 8(a) shows the trajectory in a 2D counterpropagating beam case with $l_1 = -l_2 = 1$ and $p_1 = p_2 = 0$ and Fig. 8(b) shows the corresponding projection in the xy plane. The initial position is at $\mathbf{R}_0 = 10\lambda\hat{\mathbf{x}}$ and the initial velocity components are $(0.02, 0.02, 0.05) \text{ ms}^{-1}$. Figure 9 shows the evolution of the velocity components. From Figs. 8 and 9 it can be seen that the atom is subject to friction forces from all directions, which result in it coming to rest at a point within the potential profile. We have shown earlier that the locus of the dipole potential minimum for the 2D case with $(1, 0)$ beams is in the form of two intersecting circles, satisfying Eqs. (65) and (66). This is shown in Fig. 10 for the case $w_0 = 35\lambda$. The trajectory end point for the case depicted in Figs. 8 and 9 lies on the curve shown in Fig. 10. Thus this theory assigns predetermined end points for a given ion under given initial conditions. That this is clearly the case can be seen from Table I, where the coordinates of the trajectory end point recorded for various starting points satisfy Eqs. (65) and (66) for the two intersecting circles shown in Fig. 10.

V. COMMENTS AND CONCLUSIONS

In this paper we have explored the nature of the radiation forces and their influence on atomic motion for a specific type of laser light, namely, Laguerre-Gaussian laser light in the form of a single beam and for multiple beams in various configurations. We have emphasized from the outset that the orbital angular momentum effects characterizing these modes give rise to different physical phenomena when such

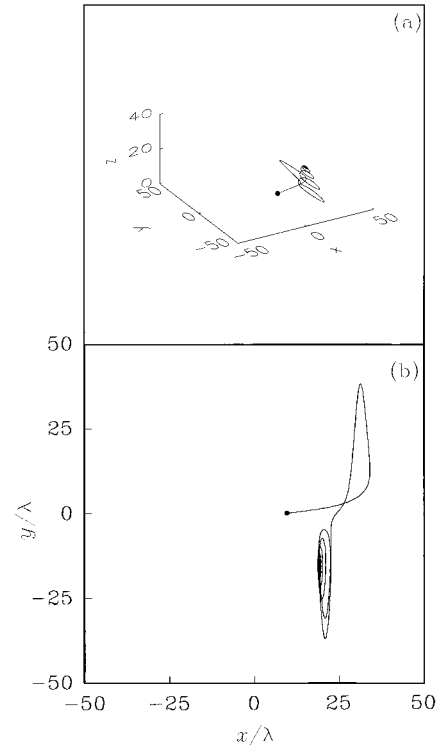


FIG. 8. (a) Trajectory of a Mg^+ ion in 2D counterpropagating LG beams involving two orthogonal pairs: one pair has the z axis as a common axis with $l_1 = -l_2 = 1$ and $p_1 = p_2 = 0$ and the second pair has the y axis as a common axis and $l_3 = -l_4 = 1$ and $p_3 = p_4 = 0$. All distances are in units of the wavelength of the light λ . The initial position of the Mg^+ ion is at $\mathbf{R}_0 = 20\lambda\hat{\mathbf{x}}$ and the initial velocity components are $(0.02, 0.02, 0.05) \text{ ms}^{-1}$. (b) Projection in the xy plane of the trajectory in (a).

light is made to interact with atoms at near resonance. We have shown that a variety of forces come into play when the LG light is arranged in well-defined multiple beams particularly linear, orthogonal 2D, and symmetric coplanar three-beam configurations. We have, for simplicity, considered only coaxial multiple LG beams of the same kind whose beam waists coincide and have assumed that all counterpropagating pairs have the same magnitude of orbital angular momentum quantum numbers l and p . Notwithstanding the simplification inherent in these symmetric configurations, the physics has been intricate, but has given rise to effects associated with the orbital angular momentum of LG beams.

The results show that LG light generates a potential arising from the dipole force, while the dissipative force provides a mechanism to cool the atom axially and that there is a torque that can be utilized to cool or heat the azimuthal motion. Furthermore, there are reciprocating forces involving an interplay between motions in orthogonal directions that can generate oscillatory and precessional motions.

The model we have adopted involves linearly polarized light. We have also assumed that the beams are independent and possess no fixed phase relationship, thus excluding interference or multiphoton processes [1], for example, absorption from one beam followed by emission into the other beam. The atom responds therefore to the sum of the individual forces acting upon it. This is distinct from the case in which the two counterpropagating beams form a standing

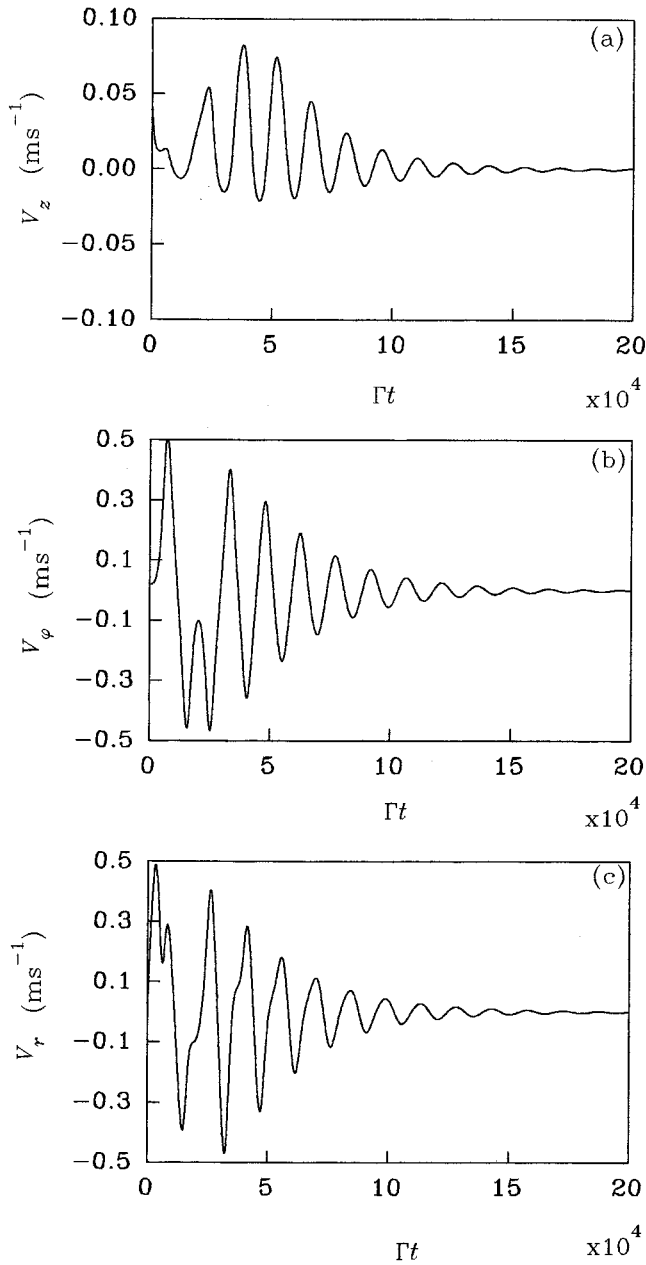


FIG. 9. Evolution of the velocity components corresponding to case with initial position at $\mathbf{R}_0=10\lambda\hat{\mathbf{x}}$ (a) $V_z(t)$, (b) $V_\phi(t)$, and (c) $V_r(t)$. Note that all components of velocity go to zero after a sufficiently long time.

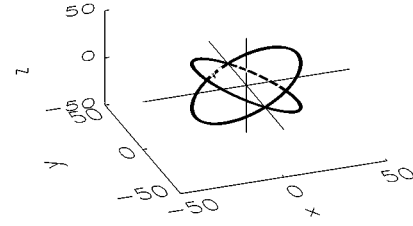


FIG. 10. Locus of spatial points where the dipole potential profile due to a system of two orthogonal pairs of counterpropagating LG beams possesses the lowest minimum. All distances are in units of the wavelength of the light λ .

wave and the possible Doppleron effects [1] that can arise under such circumstances. Work on the case of a standing LG wave is planned to be reported elsewhere.

In summary, this paper has dealt with the basic features that can arise when an atom interacts with multiple Laguerre-Gaussian beams possessing orbital angular momentum. The main effects of LG light on atomic behavior are elucidated for the 1D counterpropagating beams where we find reciprocity between axial and azimuthal motions and the existence of a static torque and a characteristic dipole potential. In the case of 2D counterpropagating beams the potential profile indicates that cooled atoms are forced to congregate into well-defined loci depending on the size of the light beams. Initial cooling need not be effected by the same LG beams; the primary aim of the LG beams at the late cooling stages could be the installation of the dipole potential; artificially generated dark field beams have been experimentally exploited [21]. We have illustrated the results by considering the case of beams of order of tens of wavelengths diameter. This results in atoms sitting on loci separated by distances of tens of wavelengths. However, the generation of results for diameters of order of millimeters is straightforward and would lead to atomic loci separated by distances in the mms scale. We have also briefly considered the loci for the 3D case and for the three coplanar converging LG beams. For these cases no solutions of the dynamical equation were presented and we have only pointed out the characteristic potential profiles and the points at which cooled atoms would congregate.

The effects of orbital angular momentum have been discussed here in connection with Laguerre-Gaussian modes. It

TABLE I. Coordinates x_f, y_f, z_f of the trajectory end points against initial coordinates x_0, y_0, z_0 . All distances are in units of the wavelength of the light λ . The last three columns demonstrate that the ion end points always lie on the two intersecting circles shown in Fig. 10.

| x_0 | y_0 | z_0 | x_f | y_f | z_f | $\sqrt{x_f^2 + y_f^2}$ | $\sqrt{y_f^2 + z_f^2}$ | $w_0/\sqrt{2}$ |
|-------|-------|-------|--------|-------|--------|------------------------|------------------------|----------------|
| 20 | 0 | 0 | 15.96 | 18.92 | 15.96 | 24.75 | 24.75 | 24.75 |
| 20 | 20 | 0 | 2.84 | 24.61 | 2.84 | 24.75 | 24.75 | 24.75 |
| -20 | 20 | 10 | -14.27 | 20.22 | 14.27 | 24.75 | 24.75 | 24.75 |
| -20 | 20 | -10 | -13.81 | 20.54 | -13.81 | 24.75 | 24.75 | 24.75 |

appears likely, however, that the dynamically induced stabilization of the atomic motion, the so-called supermolasses configuration, which arises from a small displacement of the molasses fields [22], can be related to the azimuthal forces arising from orbital angular momentum, as probably can the macroscopic vortex force due to the offset beams in the spin-polarized spontaneous force-atom trap of Walker *et al.* [23]. As we have shown, the orbital angular momentum of the Laguerre-Gaussian modes is explicit and their influence on

atomic motion is more straightforward to interpret.

ACKNOWLEDGMENTS

The authors are grateful to Dr. E. Riis and Dr. R. C. Thompson for useful discussions. This work was carried out under EPSRC Grant No. GR/J64009, which also provided support for W.K.L. and V.E.L. L.A. was working at JILA, University of Colorado during the preparation of the paper.

-
- [1] V. S. Letokhov and V. G. Minogin, *Laser Light Pressure on Atoms* (Gordon and Breach, New York, 1987).
- [2] A. P. Kazantsev, G. I. Surdutovich, and V. P. Yakovlev, *Mechanical Action of Light on Atoms* (World Scientific, Singapore, 1990).
- [3] W. D. Phillips, in *Fundamental Systems in Quantum Optics*, Proceedings of the International School of Physics, Les Houches, Session LIII, 1990, edited by J. Dalibard, J.-M. Raimond, and J. Zinn-Justin (Elsevier, Amsterdam, 1992).
- [4] H. Metcalf and P. van der Straten, *Phys. Rep.* **244**, 203 (1994).
- [5] A. Ashkin, *Phys. Rev. Lett.* **24**, 156 (1970); **25**, 1321 (1970).
- [6] D. Wineland and H. Dehmelt, *Bull. Am. Phys. Soc.* **20**, 637 (1975); T. Hansch and A. Schawlow, *Opt. Commun.* **13**, 68 (1975).
- [7] S. Chu, J. E. Bjorkholm, A. Ashkin, and A. Cable, *Phys. Rev. Lett.* **57**, 314 (1986).
- [8] L. Allen, M. W. Beijersbergen, R. J. C. Spreeuw, and J. P. Woerdman, *Phys. Rev. A* **45**, 8185 (1992).
- [9] M. W. Beijersbergen, L. Allen, H. E. L. O. van der Veen, and J. P. Woerdman, *Opt. Commun.* **96**, 123 (1993); S. M. Barnett and L. Allen, *ibid.* **110**, 670 (1994); S. J. van Enk and G. Nienhaus, *ibid.* **94**, 147 (1992).
- [10] L. Allen, V. E. Lembessis, and M. Babiker, *Phys. Rev. A* **53**, R2937 (1996).
- [11] W. L. Power, L. Allen, M. Babiker, and V. E. Lembessis, *Phys. Rev. A* **52**, 479 (1995); M. Babiker, L. Allen, and W. L. Power, *Phys. Rev. Lett.* **73**, 1239 (1994); L. Allen, M. Babiker, and W. L. Power, *Opt. Commun.* **112**, 141 (1994).
- [12] R. J. Cook, *Phys. Rev. A* **20**, 224 (1979).
- [13] J. Dalibard and C. Cohen-Tannoudji, *J. Phys. B* **18**, 1661 (1985).
- [14] H. A. Haus, *Waves and Fields in Optoelectronics* (Prentice-Hall, Englewood Cliffs, NJ, 1984).
- [15] C. Cohen-Tannoudji, J. Dupont-Roc, and G. Grynberg, *Atom-Photon Interactions: Basic Processes and Applications* (Wiley Interscience, New York, 1975).
- [16] H. C. Torrey, *Phys. Rev.* **76**, 1059 (1949).
- [17] L. Allen and J. H. Eberly, *Optical Resonance and Two-Level Atoms* (Wiley Interscience, New York, 1975).
- [18] H. Al-Hilfy and R. Loudon, *Opt. Acta* **32**, 995 (1985).
- [19] G. Grynberg, B. Lunis, P. Verkerk, J.-Y. Courtis, and C. Salomon, *Phys. Rev. Lett.* **70**, 2249 (1993).
- [20] M. Babiker, V. E. Lembessis, W. K. Lai, and L. Allen, *Opt. Commun.* **123**, 523 (1996).
- [21] M. H. Anderson, W. Petrich, J. R. Ensher, and E. A. Cornell, *Phys. Rev. A* **50**, R3597 (1994).
- [22] S. Chu, M. G. Prentiss, A. Cable, and J. Bjorkholm, in *Laser Spectroscopy VII*, edited by W. P. Person and S. Svanberg (Springer-Verlag, Berlin, 1987); V. S. Banato, N. Bigelow, G. I. Surdutovitch, and S. Zilio, *Opt. Lett.* **19**, 1568 (1994).
- [23] T. Walker, P. Feng, D. Hoffman, and R. S. Williamson III, *Phys. Rev. Lett.* **69**, 2168 (1992).